

Simplifying Energy Optimization using Partial Enumeration

Carl Olsson

Johannes Ullén

Yuri Boykov

Centre for Mathematical Sciences

Lund University, Sweden

calle@maths.lth.se

ulen@maths.lth.se

Department of Computer Science

University of Western Ontario, Canada

yuri@csd.uwo.ca

Abstract

Energies with higher order non-submodular interactions have been shown to be very useful in vision due to their high modeling power. Optimization of such energies, however, is generally NP-hard. One naive approach that works for small problem instances is exhaustive search, that is, enumeration of all possible labelings of the underlying graph. We propose a general approach for minimizing complex high-order energies on large graphs that is based on enumeration of labelings of certain small subsets.

We show how to benefit from such partial enumerations by equivalently reformulating the optimization problem on a new graph. Each node of this graph represents a subset of pixels with feasible labels (node states) corresponding to enumeration of this subset. If pixel subsets are chosen as an overlapping partition of the image then our partial enumeration approach simplifies the original high-order energy optimization to a pairwise interaction problem that can be efficiently solved by methods like TRW-S. We demonstrate that our approach often yields the exact global minimum (zero duality gap) for some high-order (curvature) and non-submodular (deconvolution) energies known to be difficult.

1. Introduction

Discrete optimization of MRF models is of fundamental importance for many early vision problems. The ability to compute optimal or guaranteed near optimal solutions in polynomial time makes them suitable for a large class of problems. Applications include stereo-matching, segmentation, superresolution and deconvolution [1, 13].

There are many approaches to solving these problems. When the energy consists of pairwise submodular interactions it can be minimized exactly in polynomial time using max-flow/min-cut algorithms [1].

In case of non-submodular interactions one of the most successful methods is roof duality [13]. The idea is to compute a lower bound on the optimal energy in polynomial

time using graph methods. If the lower bound is not tight roof duality provides partial solutions, that is, identifies subsets of pixels for which the optimal label can be determined. To compute a different lower bound Fix *et al.* [3] propose to discard edges of the original graph until only a tree (or a low tree-width graph) remain. The resulting energy can be optimized efficiently using dynamic programming.

Recently researchers have started to consider optimizing energies with higher order interactions. A common approach for solving these problems are reduction techniques, e.g. [4, 5], where a higher order clique is replaced by a set of pairwise interactions by introducing auxiliary nodes. A generalization of roof duality (GRD) to cliques of order 3 and 4 was presented in [7].

A particular application with 4th order interactions that has received a lot of attention recently is segmentation with curvature regularization. In [15] a linear programming formulation is used to compute tight lower bounds of the energy. Shekhovtsov *et al.* [16] learns a set of model patches with low curvature and then attempts to encourage assignments of pixels that agree with these patches. The resulting energy roughly penalizes the curvature of the selected model patch and quality of fit to the patch, that is, the difference between the model patch and the pixel assignments.

For problems with non-binary labels state-of-the-art methods are based on message passing over trees [8, 10]. These methods compute a lower bound on the original problem by decomposing the energy over subtrees and optimizing these independently using message passing. In [9] the dual decomposition scheme is extended to energies with higher order interactions. The problem is decomposed into sub problems that can be solved using message passing. A solution to the original problem is extracted by combining the solutions of the subproblems.

1.1. Contributions and Related Work

In this paper we demonstrate how to reformulate energies (both pairwise and higher order), by enumerating all labelings of small subsets of pixels, so that optimization becomes easier. We show how it is possible to strengthen

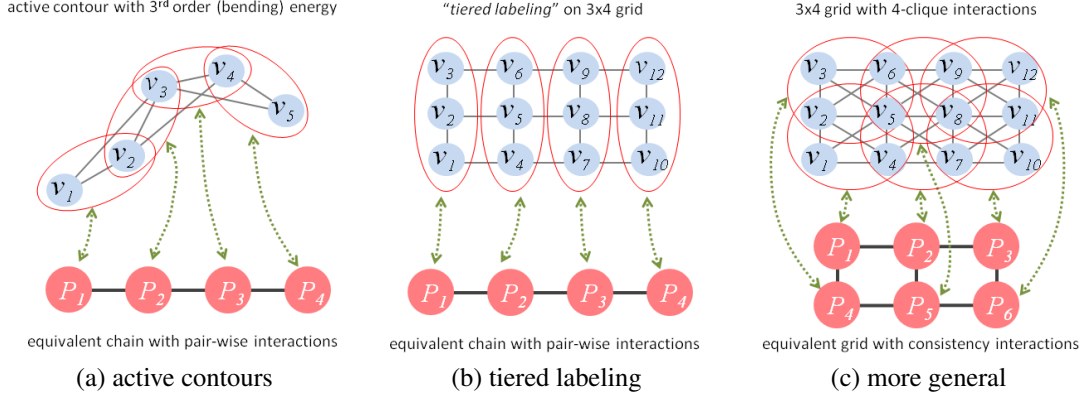


Figure 1: Examples of *partial enumeration* in optimization. Some instances of partial enumeration can be found in prior art: 3-rd order active contour model and *tiered labeling* energy on a grid [2] are reduced to pairwise energies on a chain that can be optimized by dynamic programming (a-b). We propose partial enumeration as a general approach simplifying optimization of complex (non-submodular or high-order) energies, e.g. see (c).

the lower bounds provided by standard algorithms such as [8] using this kind of *partial enumeration*. Specifically, we group pixels into overlapping patches in a sliding window fashion, see Fig.1(c), and enumerate the states and costs for each patch. We then equivalently reformulate the same energy on a new graph, where each node corresponds to a patch and its labels correspond to the enumerated states. Note that if overlapping patches are large enough to cover all cliques in the original energy, then state enumeration allows to convert all arbitrarily complex (e.g. non-submodular or high-order) interactions into unary potentials in the reformulated energy. Such a significant simplification can not come for free. First of all, the label space for each node (patch P) of the new graph includes all *partial labelings* \mathcal{L}^P . This is much larger than the set of labels \mathcal{L} for each pixel in the original graph. Moreover, it is necessary to introduce *consistency constraints* for each pair of overlapping patches since the corresponding two partial labelings should agree in the overlap region. The new graph will have pairwise interactions and can therefore be optimized using standard methods such as TRW-S [8]. We show that this procedure generates stronger bounds than state-of-the-art methods do when using the original graph formulation. Additionally it enables solving problems with higher order interactions using standard methods such as [8, 10].

Related work: Interestingly, some specific examples of partial enumeration could be found in prior art. For example, to optimize a *snake* with bending (3-clique) energy it is customary to combine each pair of adjacent control points into a single super-node, see Fig.1(a). The number of states for each super-node is m^2 if m is the number of allowed states for each control point. However, the higher-order bending energy on the original snake reduces to a pair-wise

energy on the chain of super-nodes. Despite increase of the label space, this problem can be very efficiently solved with dynamic programming in $O(nm^3)$. A similar reduction to dynamic programming is used for MRF optimization in [2] where high-order interactions are due to *tiered labeling* constraints. This approach can also be seen as special case of partial enumeration, even though non-overlapping “patches” are sufficient in their case, see Fig.1(b).

We present partial enumeration as a general approach for simplifying MRF labeling problems using overlapping patches to reduce complex interactions to unary potentials. Jung et al. [6] also use patches to simplify complex potentials. They iterate by randomly sampling patches of some small size. Once some patch is selected, they minimize the energy within that patch (using enumeration or dynamic programming, if possible) while assignment of all other graph nodes is fixed. This could be seen as a patch-based extension of ICM algorithm. In contrast, we optimize over all patches simultaneously.

2. Framework

For simplicity we will start by assuming that our energy consists of pairwise interactions on a regular 4-connected pixel grid. We represent this grid using a graph $\mathcal{G} = (\mathcal{V}, \mathcal{E})$, where \mathcal{V} are the nodes (pixels) and \mathcal{E} are the edges. To each edge we associate an interaction cost $E_{ij}(x_i, x_j)$. We assume that this cost is positive but not necessarily submodular. Our energy is now

$$E^{\mathcal{G}}(\mathbf{x}) = \sum_{(i,j) \in \mathcal{E}} E_{ij}(x_i, x_j). \quad (1)$$

The space of feasible assignments \mathcal{L} , are the binary vectors of size n , $\{0, 1\}^n$ where n is the number of nodes. The

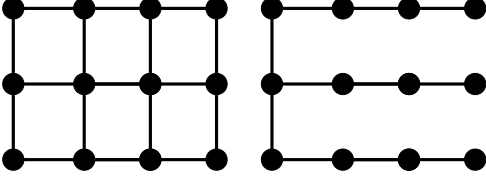


Figure 2: *Left*: 4-connected graph. *Right*: Sub-tree.

variable x_i is the assignment to node i and $\mathbf{x} \in \mathcal{L}$ is the vector containing all the node assignments.

It is well known that optimization of such energies are in general NP-hard. In the special case of an energy defined on a tree it is possible to compute the global optimum in polynomial time using, for example, message passing. Therefore researchers have successfully applied tree based algorithms for these problems. For example [8, 10] decomposes the grid into trees, optimize these and computes a lower bound on the original energy. Fix *et al.* [3] discard edges of the original graph until only a tree (or low tree-width graph) remains. In this section we will show how it is possible to use partial enumeration to strengthen these approaches.

2.1. Inference using "Super Nodes"

The intuition behind our construction is that by enumerating local interactions and encoding them into labels instead of edges it is possible to make the trees that we optimize over contain more edges from the original graph than regular subtrees. Therefore the lower bounds provided by the former trees should be stronger than the latter.

Let us first consider a subtree $\mathcal{T} = (\mathcal{V}, \mathcal{E}^{\mathcal{T}})$ of the initial graph \mathcal{G} (see figure 2). Since we have discarded edges we have

$$E^{\mathcal{T}}(\mathbf{x}) \leq E^{\mathcal{G}}(\mathbf{x}), \quad (2)$$

with equality if and only if values of the interactions at the discarded edges are all zero. Hence optimizing over this tree provides a lower bound on our original energy. The goal of our construction is now to strengthen this lower bound.

The idea is very simple: we will group neighboring nodes together into "super nodes" and enumerate all the values of the interactions between them. We start by forming patches of size 2×2 into super nodes. This is done in a sliding window fashion, that is, super node (r, c) consists of the nodes (r, c) , $(r, c + 1)$, $(r + 1, c)$ and $(r + 1, c + 1)$, where r and c are the row and column coordinates of the pixels. We call the set of super nodes $\mathcal{V}_{2 \times 2}$.

Each super node label can take 16 values corresponding to states of the individual pixels. We call the set of possible assignments for this graph $\mathcal{L}_{2 \times 2}$. The pairwise interactions of the original problem are now transformed to unary potentials since we enumerate all states within the super node.

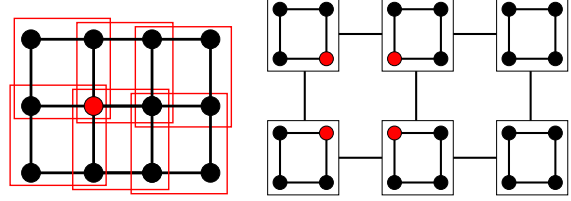


Figure 3: Supernodes are formed in a sliding window fashion. The red pixels occur in 4 of the new super nodes. Pairwise interactions between the edges ensure that shared pixels are assigned the same value in all super nodes.

Note that since patches are overlapping the edges of the original graph can be contained in up to two super nodes. In order not to change the energy we weight the new unary potentials such that the total contribution of the edges is the same as in the original graph. There are many ways of doing this, but for simplicity we give edges that occur twice the weight $1/2$.

Finally to ensure that each pixel takes the same value in all the super nodes where it is contained we add pairwise "consistency" edges $\mathcal{E}_{2 \times 2}$ between neighboring super nodes (see Figure 3). That is, label assignments where neighboring nodes assign shared pixels different values are penalized with a large value (we use 10^{14} in our implementations). Note that all super nodes that share pixels do not have a consistency edge, it is enough to use a 4-connected neighborhood structure.

The energy $E_{2 \times 2}^{\mathcal{G}}$ of the new graph $\mathcal{G}_{2 \times 2} = (\mathcal{V}_{2 \times 2}, \mathcal{E}_{2 \times 2})$ fulfills

$$\min_{\mathbf{x} \in \mathcal{L}} E^{\mathcal{G}}(\mathbf{x}) = \min_{\mathbf{x}^{2 \times 2} \in \mathcal{L}_{2 \times 2}} E_{2 \times 2}^{\mathcal{G}}(\mathbf{x}^{2 \times 2}) \quad (3)$$

by construction (assuming that the inconsistency penalty is chosen large enough). Here $\mathbf{x}^{2 \times 2}$ is the vector containing assignments of the super nodes.

2.2. Lower Bounds and Consistency of Tree-Assignments

The subtrees of $\mathcal{G}_{2 \times 2}$ has a useful property that subtrees of \mathcal{G} does not have. Namely, if optimization over a subtree of $\mathcal{G}_{2 \times 2}$ gives the correct solution then the lower bound will also be tight. The reason is that subtrees of $\mathcal{G}_{2 \times 2}$ still contain all the edges of the original graph within their (super) nodes.

Consider a subtree $\mathcal{T}_{2 \times 2} = (\mathcal{V}_{2 \times 2}, \mathcal{E}_{2 \times 2}^{\mathcal{T}})$ of $\mathcal{G}_{2 \times 2}$. We form $\mathcal{T}_{2 \times 2}$ by discarding edges from $\mathcal{G}_{2 \times 2}$. When solving

$$\min_{\mathbf{x}^{2 \times 2} \in \mathcal{L}_{2 \times 2}} E_{2 \times 2}^{\mathcal{T}}(\mathbf{x}^{2 \times 2}) \quad (4)$$

the solution might therefore violate some of the consistency constraints of $\mathcal{G}_{2 \times 2}$. We will say that an assignment $\mathbf{x}^{2 \times 2}$

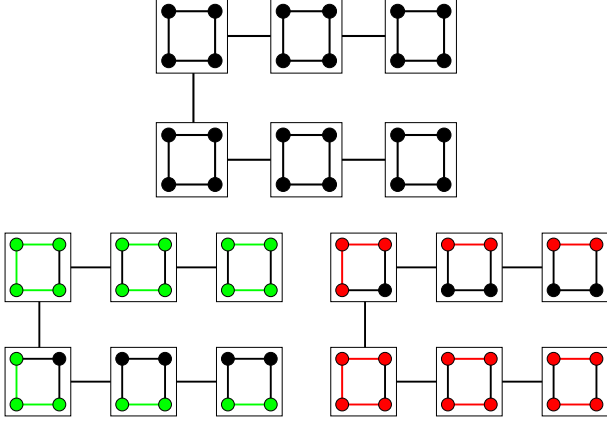


Figure 4: *Top*: A Sub tree $\mathcal{T}_{2 \times 2}$ of $\mathcal{G}_{2 \times 2}$ in Figure 3. *Bottom*: $\mathcal{T}_{2 \times 2}$ contains two copies (red and green edges) of the tree in Figure 3.

is *consistent* if all super nodes that share a pixel assigns this pixel the same value. Since such assignments do not violate any of the consistency constraints we have

$$E_{2 \times 2}^{\mathcal{T}}(\mathbf{x}^{2 \times 2}) = E_{2 \times 2}^{\mathcal{G}}(\mathbf{x}^{2 \times 2}). \quad (5)$$

Therefore, if the solution of (4) is consistent, then the lower bound given by the tree will be tight

$$\min_{\mathbf{x}^{2 \times 2} \in \mathcal{L}_{2 \times 2}} E_{2 \times 2}^{\mathcal{T}}(\mathbf{x}^{2 \times 2}) = \min_{\mathbf{x} \in \mathcal{L}} E^{\mathcal{G}}(\mathbf{x}). \quad (6)$$

The subtrees of $\mathcal{G}_{2 \times 2}$ also have the advantage that they often provide stronger lower bounds than subtrees of \mathcal{G} even if the solution is not consistent. Consider for example the subtree \mathcal{T} of \mathcal{G} in Figure 2. We can form a similar tree $\mathcal{T}_{2 \times 2}$ from $\mathcal{G}_{2 \times 2}$, see Figure 4. Looking in the super nodes of $\mathcal{T}_{2 \times 2}$ and considering the consistency edges we see that we can find two instances of \mathcal{T} within $\mathcal{T}_{2 \times 2}$ (see bottom row Figure 4) both with weights $1/2$ (here the edges that have weight 1 are allowed to belong to both trees). Hence if we view these two instances as independent and optimize them we get the same energy as optimization over \mathcal{T} would give. In addition there are other edges present in $\mathcal{T}_{2 \times 2}$, therefore the lower bound provided by this tree will be at least as good as lower bound given by \mathcal{T} .

2.3. Improving the Bound by Increasing Node Size

In case the lower bound given by $\mathcal{T}_{2 \times 2}$ is not tight we can try to improve it by making the super nodes bigger and thereby making them contain more interactions. The key observation is that if the bound is not tight, then there is an inconsistency somewhere. By concatenating patches into new super nodes we can make sure that the previous inconsistencies do not occur thereby tightening the lower bound.

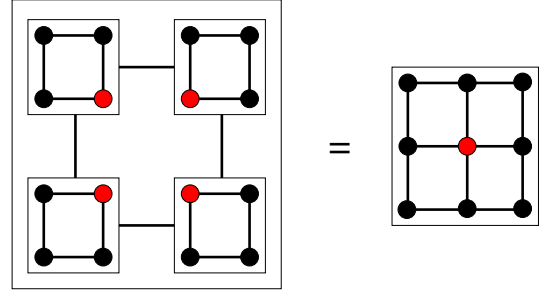


Figure 5: The nodes of $\mathcal{G}_{3 \times 3}$ are created by grouping nodes of $\mathcal{G}_{2 \times 2}$ in groups of 2×2 in a sliding window fashion. Since consistency is enforced within nodes (e.g. the red pixel is the same everywhere) the result is that each node will contain a 3×3 patch.

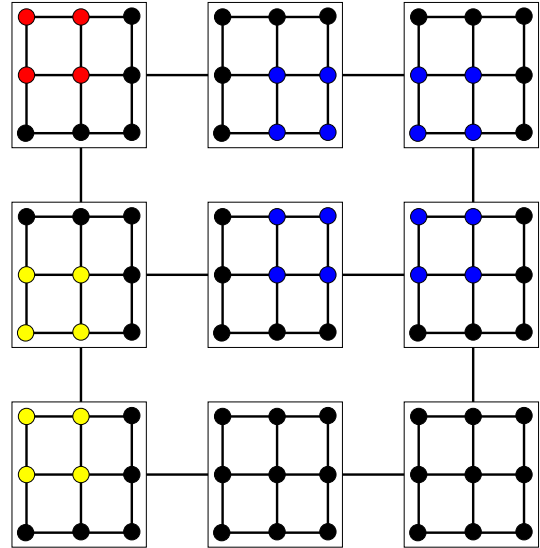


Figure 6: Tree $\mathcal{T}_{3 \times 3}$. Red patch occurs once, yellow twice and blue four times.

Therefore we group the nodes of $\mathcal{G}_{2 \times 2}$ into groups of 2×2 in a sliding window fashion. Since neighboring nodes have common pixels that are fused into one (see Figure 5), the result is graph $\mathcal{G}_{3 \times 3}(\mathcal{V}_{3 \times 3}, \mathcal{E}_{3 \times 3})$. The edge set is constructed similar to that of $\mathcal{G}_{2 \times 2}$. Note that even though three consecutive nodes will share pixels it is enough to enforce consistency using a 4-connected neighborhood. In this construction all patches except those that are at image borders will occur 4 times within the new nodes (see Figure 6). We therefore weight the costs so that their total contribution to the energy does not change.

The energy $E_{3 \times 3}^{\mathcal{G}}$ represented by the new graph fulfills

$$\min_{\mathbf{x}^{3 \times 3}} E_{3 \times 3}^{\mathcal{G}}(\mathbf{x}^{3 \times 3}) = \min_{\mathbf{x}^{2 \times 2}} E_{2 \times 2}^{\mathcal{G}}(\mathbf{x}^{2 \times 2}). \quad (7)$$

If the bound obtained from the sub tree $\mathcal{T}_{3 \times 3}$ is not tight we can recursively do the same thing again and increase it further. In this case we obtain sliding window patches of size 4×4 .

Note that in each step of increasing the patch size the graph size is reduced (by one row and one column). Therefore in the extreme case we will only have one patch and will therefore be enumerating all combinations of pixel assignments, so it is clear that the lower bound will approach the optimum.

Remark In the beginning of this section we assumed that the energy consists of pairwise interactions. However we can do the same thing for higher order interactions. The only restriction is that we start with super nodes that contain all the pixels involved in the interaction. In Section 3 we use patches of size up to 5×5 to encode higher order interactions.

3. Experiments

In this section we will test our approach of partial enumeration from Section 2. We optimize the resulting graphs using TRW-S [8]. We use different super node size depending on the size of the interactions, but we always use a 4-connected neighborhood for enforcing consistency. In all the tested cases, TRW-S with our graph construction provided a solution and a lower bound with the same energy (same up to machine precision).

3.1. Stereo

In this section we optimize the energies occurring in Woodford *et al.* [17]. The goal is to find a dense disparity map for a given pair of images. The regularization of this method penalizes second order smoothness of the disparity map. The 2nd derivative is estimated from three consecutive disparity values (vertically or horizontally). Thus, the resulting optimization problem contains 3rd-order non-submodular terms that are challenging to optimize.

To solve this problem [11] uses fusion moves. In this move two proposals are fused together into a new disparity map with lower energy. To compute the fusion move [17] first reduces the interactions to pairwise (by introducing auxiliary nodes) and applies Roof duality (RD) [13]. In contrast we decompose the problem into patches of size 3×3 , that contain entire triple cliques. Note that the interactions will occur in as many as three supernodes. We therefore weight these so that the energy does not change. Each super node consists of 9 pixels. We allow all combinations of these and therefore there are $2^9 = 512$ labels.

Table 1 shows the results for the `Cones` dataset from [14] when fusing "SegPln" proposals [17]. Starting from a randomized disparity map we fuse all the proposals. To

ensure that each subproblem is identical for the two approaches, we feed the solution from roof duality into our approach before running the next fusion. The proposals on average result in 24% unlabeled pixels when using RD. Furthermore there is a one percent relative duality gap for RD. We also tested using the "improve" heuristic [13] for completing the labeling. This gives a slight reduction in duality gap. Running probe [13] instead of improve is not feasible due to the large number of unlabeled variables.

We also compared the final energies when we run the methods independent of each other (not feeding solutions into our approach), in this case our final solution has 0.82% lower energy than that of RD with "improve".

3.2. Binary Deconvolution

In this section we test our method on binary deconvolution. Figure 7 (a) shows a circle convolved with a 3×3 mean value kernel with additional noise added to it. The goal is to recover the original (binary) image. We formulate the energy as outlined in [12]. Figure 7 (b) shows the solution obtained using RD, here the gray pixels are unlabeled. For comparison we also plotted the solution obtained when solving the the same problem as RD but with TRW-S. The solution obtained is quite poor and there is a substantial duality gap. In contrast (d) shows the solution obtained when first forming super nodes with patches of size 3×3 and then applying TRW-S. In this case there is no duality gap, so the obtained solution is optimal. To solve the super node problem takes 2.6134 seconds, in contrast the solutions provided by RD and TRW-S (with the original graph formulation) takes 0.0324 and 0.8825 seconds respectively to compute.

3.3. Curvature

Next we apply our framework to segmentation with curvature regularization. Throughout this section we will use approximations of the energy

$$E(S) = \int_{\text{int}(S)} c_{\text{int}}(x) dx + \int_{\text{ext}(S)} c_{\text{ext}}(x) dx + \int_{\partial S} \lambda |\kappa| d\sigma, \quad (8)$$

where $c_{\text{int}}(x)$ and $c_{\text{ext}}(x)$ is the cost of assigning pixel x to interior and exterior respectively, κ is the curvature and λ is the weight of the regularization. We use absolute curvature since it does not have any growing bias, but in principle any other version could be used.

First, we consider a very coarse approximation of curvature on a 4-connected grid. In this case we only allow boundary edges that are either horizontal or vertical and, therefore, patches of size 2×2 are enough to approximate the curvature of such boundaries. Figure 8 shows 4 of the 16 patch states used to encode curvature (the others are rotations and inversions of these). Figure 9 compares the results



(a) Cones.

	Energy	Lower bound	Relative gap	Time (s)
Our	1.4558e+10	1.4558e+10	1.4471e-14	315.3342
RD	1.4637e+10	1.4518e+10	9.3694e-3	1.9216
Our/Rd	0.9958	1.0019	4.3825e-13	180.6859

(b) Average results of proposal fusing on Cones.

Table 1: After RD on average 39713 out of 168750 variables where unlabeled. Relative gap is defined as (Energy-Lower bound)/Lower bound. "Improve" was also tested after RD, lowering the average Energy for RD to 1.4609e+10.

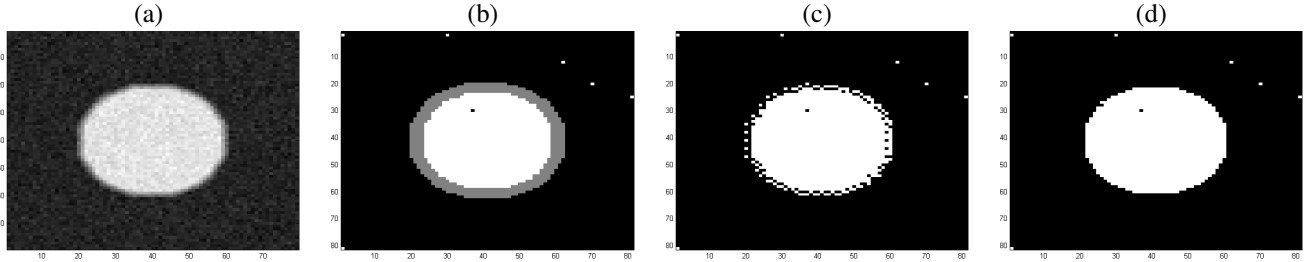


Figure 7: Binary Deconvolution. (a) - Convolved image with added noise. (b) - Solution provided by RD. Gray pixels are unlabeled. (c) - Solution obtained by optimizing the pairwise energy (without forming patches) with TRW-S. The energy of this solution is 24.0214 and the lower bound provided by TRW-S is -11.7096 . (d) - Solution obtained from TRW-S when using patches of size 3×3 . The energy of this solution is 15.531330 and the lower bound provided by TRW-S is also 15.531330.

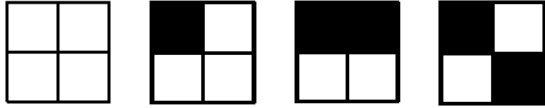


Figure 8: Four patch states used for encoding 4-connected curvature. The penalties for the patches are 0 , $\pi/2$, 0 and π respectively.

of our curvature-based and more standard length-based regularizations. Curvature regularization preserves thin elongated vertical and horizontal structures while suppressing the noise. In contrast, length regularization can not preserve thin objects and suppress noise at the same time.

Figure 10 compares our approach to Generalized Roof Duality [7] for different levels of regularization. GRD only labels pixels for very moderate levels of regularization. In contrast, our approach provides globally optimal solutions with no duality gap.

3.3.1 Better Approximation of Curvature

For patches of size 2×2 it is only possible to encourage horizontal and vertical boundaries. For example, along a diagonal boundary edge all 2×2 patches look like the sec-

ond patch in Figure 8. To make the model more accurate and include directions that are multiples of 45 degrees we can increase the size of the patches. For multiples of 45 degrees it is enough to have 3×3 patches and for 22.5 degrees we use patches of size 5×5 . However, the number of distinct patch-labels needed to encode the interactions (transitions between directions) is quite high. It is not feasible to determine their costs by hand (as in 2×2 case).

To compute the specific label costs we generate representative windows of size slightly larger than the patch (for 3×3 patches we use 5×5 windows) that contain either a straight line or a transition between two directions of known angle difference, i.e. curvature, see Fig. 11. From this window we can determine which super node assignments occur in the vicinity of different transitions. We extract all the assignments and constrain their sum to be the known curvature of the window. Furthermore, we require that the cost of each label is positive. If a certain label is not present in any of the windows we do not allow this assignment. This gives us a set of linear equalities and inequalities for which we can find a solution (using linear programming). The procedure gives 122 and 2422 labels for the 3×3 and 5×5 cases respectively.

The approach of modeling curvature with patches is somewhat related to the idea of [16] (however the optimization is completely different).

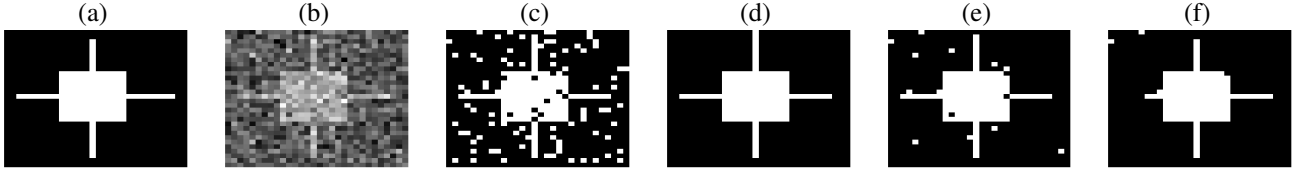


Figure 9: Curvature may potentially preserve long thin structures in contrast to length. (a) - Original image, (b) - Image with added noise, (c) - Thresholded solution, (d) 4-connected curvature regularization, (e) Length regularization with weights selected as to preserve the thin structure, (f) Length regularization with slightly larger regularization.



λ	TRW-S Energy	TRW-S Lower bound	Unlabeled by GRD(-heur)	TRW-S running time	GRD(-heur) running time
10^{-4}	4677	4677	0% (0%)	0.6620s	2496s (11.09s)
10^{-3}	4681	4681	0.2% (0.2%)	0.8818s	2001s (9.63s)
10^{-2}	4714	4714	2.7% (4.1%)	1.3187s	2324s (24.23s)
10^{-1}	4959	4959	100% (100%)	4.2875s	2334s (31.71s)
10^0	5972	5972	100% (100%)	21.7286s	2415s (25.55s)
10^1	7815	7815	100% (100%)	20.4373s	2242s (23.71s)

Figure 10: Our results for 4-connected curvature with different regularization weight λ (top row of images). TRW-S with super nodes gives a tight lower bound. GRD only labels nodes for low regularization weight (the figures within parenthesis are results when using the heuristics proposed for speedup in [7]).



Figure 11: Seven of the 5×5 windows used for computing patch costs for 3×3 curvature. (The rest are obtained as rotations, reflections of the patches and inversions of the pixel assignments).

Figures 12 and 13 show the effects of using the different regularizations. In Figure 12 we took an image of a circle and segmented it using 3 types of approximating patches. Note that there is no noise in the image, so simply truncating the data term would give the correct result. We segment this image using a high regularization weight ($\lambda = 20$ in all three cases). In (b) horizontal and vertical boundaries are favored since these have zero regularization cost. In (b) and (c) the number of directions with zero cost is increased and therefore the approximation improved with the patch size. Computing these segmentations takes 1.46, 8.94 and 55.63 seconds for (a),(b) and (c) respectively. In the case of 5×5 patches the enumeration takes a large portion of time (in fact, only 14.91 seconds is spent in TRW-S). Fig-

ure 13 shows segmentations with the different patch sizes. To compute these results we used different regularization weight ($\lambda = 1, 0.2, 0.1$ for patch size $2 \times 2, 3 \times 3$ and 5×5 respectively). The same effects are visible here. The computation times are 27.74, 36.91 seconds for patch size 2×2 and 3×3 respectively. The 5×5 version seems to be much more difficult to solve and requires almost 30 minutes of computation. (Out of this 15 minutes is enumeration.)

References

- [1] Y. Boykov, O. Veksler, and R. Zabih. Fast approximate energy minimization via graph cuts. *IEEE Transactions on Pattern Analysis and Machine Intelligence*, 2001. 1
- [2] P. F. Felzenszwalb and O. Veksler. Tiered scene labeling with dynamic programming. In *IEEE Conf. on Computer Vision and Pattern Recognition*, 2010. 2
- [3] A. Fix, J. Chen, E. Boros, and R. Zabih. Approximate mrf inference using bounded treewidth subgraphs. In *European Conf. on Computer Vision*, 2012. 1, 3
- [4] D. Freedman and P. Drineas. Energy minimization via graph cuts: Settling what is possible. In *IEEE conf. on Computer Vision and Pattern Recognition*, 2005. 1

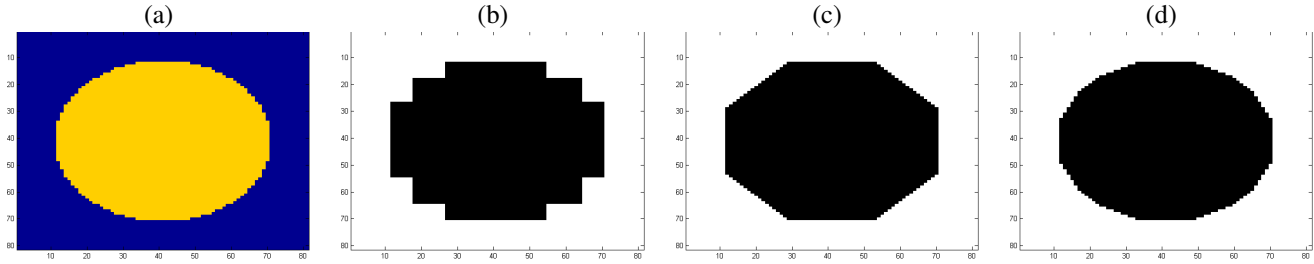


Figure 12: Segmentation results using different patch sizes with same very high regularization weight ($\lambda = 20$). (a) - Data term, (b) - 2×2 patches clearly favors horizontal and vertical boundaries, (c) - 3×3 patches, favors directions that are multiples of 45 degrees, (d) 5×5 patches, favors directions that are multiples of 22.5 degrees.



Figure 13: Segmentation of the camera man using (from left to right) 2×2 , 3×3 and 5×5 patches.

- [5] H. Ishikawa. Transformation of general binary mrf minimization to the first-order case. *IEEE Trans. Pattern Anal. Mach. Intell.*, 33(6):1234–1249, 2011. 1
- [6] K. Jung, P. Kohli, and D. Shah. Local rules for global map: When do they work? In *Annual Conference on Neural Information Processing Systems*, 2009. 2
- [7] F. Kahl and P. Strandmark. Generalized roof duality. *Discrete Applied Mathematics*, 160(16-17):2419–2434, 2012. 1, 6, 7
- [8] V. Kolmogorov. Convergent tree-reweighted message passing for energy minimization. *IEEE Trans. Pattern Anal. Mach. Intell.*, 28:1568–1583, October 2006. 1, 2, 3, 5
- [9] N. Komodakis and N. Paragios. Beyond pairwise energies: Efficient optimization for higher-order mrfs. In *IEEE Conf. on Computer Vision and Pattern Recognition*, 2009. 1
- [10] N. Komodakis, N. Paragios, and G. Tziritas. Mrf optimization via dual decomposition: Message-passing revisited. In *International Conference on Computer Vision*, 2007. 1, 2, 3
- [11] V. S. Lempitsky, C. Rother, S. Roth, and A. Blake. Fusion moves for markov random field optimization. *IEEE Trans. Pattern Anal. Mach. Intell.*, 32(8):1392–1405, 2010. 5
- [12] A. Raj and R. Zabih. A graph cut algorithm for generalized image deconvolution. In *In ICCV*, 2005. 5
- [13] C. Rother, V. Kolmogorov, V. S. Lempitsky, and M. Szummer. Optimizing binary mrfs via extended roof duality. In *IEEE conf. on Computer Vision and Pattern Recognition*, 2007. 1, 5
- [14] D. Scharstein and R. Szeliski. High-accuracy stereo depth maps using structured light. In *IEEE conf on Computer Vision and Pattern Recognition*, volume 1, 2003. 5
- [15] T. Schoenemann, F. Kahl, S. Masnou, and D. Cremers. A linear framework for region-based image segmentation and inpainting involving curvature penalization. *International Journal of Computer Vision*, 2012. 1
- [16] A. Shekhovtsov, P. Kohli, and C. Rother. Curvature prior for MRF-based segmentation and shape inpainting. In *DAGM*, 2012. 1, 6
- [17] O. Woodford, P. Torr, I. Reid, and A. Fitzgibbon. Global stereo reconstruction under second order smoothness priors. In *IEEE Transactions on Pattern Analysis and Machine Intelligence*, 2009. 5